designs

MDPI

Article

Design of a Recommender System with Safe Driving Mode Based on State-of-Function Estimation in Electric Vehicle Drivetrains with Battery/Supercapacitor Hybrid Energy Storage System

Farshid Naseri [1,*], Sepehr Karimi [2], Ebrahim Farjah [2] and Peyman Setoodeh [2,3]

[1] Electrical Energy Technology, Department of Electrical and Computer Engineering, Aarhus University, 8200 Aarhus, Denmark
[2] Department of Power and Control Engineering, School of Electrical and Computer Engineering, Shiraz University, Shiraz 71964-84334, Iran
[3] Department of Mechanical Engineering, McMaster University, Hamilton, ON L8S 4L7, Canada
* Correspondence: fna@ece.au.dk

Abstract: The performance of electric vehicle (EV) drivetrains depends on the power capability of individual components, including the battery pack, motor drive, and electric motor. To ensure safety, maximum power must be limited by considering the constraint of the weakest component in the drivetrain. While there exists a large body of work that discusses state-of-power (SoP) estimation for individual components, there is no work that considers all the components' limiting factors at once. Moreover, research on how to use these limits to adjust the performance at the system level has been rare. In this paper, the SoPs of the components are used to estimate the state-of-function (SoF) of the EV drivetrain. The SoF is defined as the maximum charge/discharge power that can be sourced and/or sunk by the drivetrain without violating the safety limits of its components. The component-level SoP estimations are fulfilled using several digital algorithms based on recursive least-squares (RLS) and Kalman filters (KFs), as well as by taking into account specific limiting conditions such as high driving altitude and ambient temperatures. An EV driven by a hybrid energy storage system based on a battery/supercapacitor, and a permanent-magnet synchronous motor is considered the use case. Based on the drivetrain SoF estimation, we propose two de-rating schemes to ensure that the drivetrain safety limits will be respected: adaptive cruise control and adaptive adjustment of pedal sensitivity. The de-rating schemes are introduced to a so-called recommender system that is implemented in MATLAB/STATEFLOW. The recommender system provides advisory feedback to the driver to switch to a different driving mode to ensure safety. The simulation results over a standard drive cycle using MATLAB/SIMULINK and STATEFLOW show the effectiveness of the proposed design at both component and system levels. The paper also proposes an implementation concept for the integration of the proposed recommender system into the advanced driver assistance system (ASAS).

Keywords: hybrid energy storage system; electric vehicle; battery; supercapacitor; state-of-function; state estimation; state-of-power (SoP); recommender system

check for updates

Citation: Naseri, F.; Karimi, S.; Farjah, E.; Setoodeh, P. Design of a Recommender System with Safe Driving Mode Based on State-of-Function Estimation in Electric Vehicle Drivetrains with Battery/Supercapacitor Hybrid Energy Storage System. *Designs* **2023**, *7*, 25. https://doi.org/10.3390/designs7010025

Academic Editors: Eric Cheng and Junfeng Liu

Received: 14 December 2022
Revised: 17 January 2023
Accepted: 28 January 2023
Published: 1 February 2023

Copyright: © 2023 by the authors. Licensee MDPI, Basel, Switzerland. This article is an open access article distributed under the terms and conditions of the Creative Commons Attribution (CC BY) license (https://creativecommons.org/licenses/by/4.0/).

1. Introduction

Transportation is responsible for about 22% of CO_2 emissions worldwide, and within this, 74% is produced by road vehicles [1]. Electrification of transportation has been considered an effective pathway to cut these emissions [2]. Electric vehicles (EVs) have gained increasing attention over the past years, and large funding has been secured worldwide to improve their marketability [3]. There have also been political efforts to improve their market share. For instance, the European Commission (EU) has announced an effective ban

on the sale of internal combustion engine cars effective from 2035 [4]. Compared to internal combustion engine (ICE)-based cars that have been driven on roads for decades with technology and reliability that have been proven, the EVs are a new technology; for them, meeting various functional safety requirements is critical. Therefore, it is also important to monitor their performance continuously.

In EV drivetrains, energy/power will be supplied from an energy storage system (ESS), and it will go through several conversion units to transform electric power from DC to AC (motor drive/inverter) and electric power to mechanical power (electric motor), and to adjust the mechanical torque at the wheels through the transmission system [5]. The drivetrain components work in synergy to propel the vehicle and to ensure road safety; it is worthwhile to monitor them continuously. The performance and capability of drivetrain components can be affected by several factors, e.g., the environmental and driving conditions such as air temperature or driving altitude that could cause lower cooling effectiveness, aging and degradation, and early failures [6–8]. The ESS can also be impacted by different charging/discharging rates during EV acceleration and/or braking and by the depth-of-discharge (DoD), e.g., when it is discharged to very low state-of-charge (SoC) levels. At the system level, it is thus important to operate the drivetrain within boundaries that will ensure the safety of all components. The drivetrain loadability should be determined based on the weakest component in the system. This information can be used to determine the maneuverability of the EV on the road, e.g., if the driver needs to adopt a particular driving mode to maintain safety. This paper puts forward the concept of "state-of-function," or SoF, for the EV drivetrain. Here, the drivetrain SoF is defined as a dynamic limit that, if respected by the electronic control unit (ECU), will ensure the safety of all individual components concurrently. While having this system-level target, in this paper, we consider a bottom-up approach wherein monitoring algorithms based on the state of the art (SotA) and some of the authors' previous research work are developed for individual components to estimate their state-of-power (SoP). A brief review of the SotA is provided in the following.

Several methods have been proposed in the literature regarding state estimation in individual EV components, e.g., Lithium-ion (Li-ion) batteries, supercapacitors, hybrid battery/supercapacitor systems, and inverters. For each component, the SoP should be estimated within a pre-determined horizon, and the idea is to make sure that with the obtained discharge power limits, the safety-related thresholds of the components such as the voltage, current, or SoC limits will not be violated. Regarding Li-ion battery power prediction, a well-established method has been proposed in [9], where power limits are calculated based on the voltage, current, and SoC limits, as well as simple battery equivalent circuit models (ECMs). This approach has been used along with other SoC estimation algorithms to improve the prediction accuracy, e.g., by using the Kalman filter [10], the unscented Kalman filter (UKF) [11,12], and the extended Kalman filter (EKF) [13]. Battery power prediction based on a predictive nonlinear model has been obtained in [14], wherein the limits on the operating temperature of the battery have been considered in addition to the limits on voltage, current, and SoC. In [15], an extremum learning algorithm has been used to estimate the SoP based on a first-order RC model. In [16], a long-term power demand prediction model is established and combined with a two-step state estimation algorithm to estimate the SoP. Similar algorithms have also been applied to predict the SoP in supercapacitor-based ESSs [1,17].

Derating electrical motors and motor drives based on power limits has been discussed in various studies in the literature. The existing derating methods are normally applied in two different scenarios: 1—under stressed operating conditions of the converter/motor, e.g., when cooling is insufficient [18,19]; 2—under abnormal conditions, e.g., when one/some of the switches in the DC–AC motor drive fails, and the converter has to be operated in a fault-tolerant mode [20–22]. These methods include techniques, for example, to directly detect a faulty operation such as an open-switch fault in the motor drive or to estimate the junction temperatures of an insulated gate bipolar transistor (IGBT) or

diodes in the converter as a key signature to detect the loadability [23]. The main aspect with which this paper distinguishes itself is the system-level estimation of the drivetrain cyclability using a new index, herein named the drivetrain's SoF. The main contributions of this paper are listed in the following:

- This paper extends the definition of the SoF for the whole EV drivetrain and estimates it at the system level (traditionally SoF has been used only with electrochemical batteries [24] and supercapacitors [25–27]). The SoF determines the maximum power and torque that can be transmitted to EV wheels such that the safety constraints of individual components are respected.
- According to the real-time value of the estimated EV SoF and the real-time road load conditions, two derating schemes are proposed, namely the adaptive cruise control and adaptive pedal sensitivity adjustment. The derating schemes provide safer driving conditions for the system components and the whole EV.
- The SoF estimation subroutine and the derating schemes are designed and implemented as part of an efficient online recommender system, which can be embedded into the advanced driver assistant system (ADAS) of the EV to provide better intelligence, autonomy, and flexibility. When necessary, the proposed recommender system interacts with the driver and may recommend a particular performance mode depending on recent state estimation results.

The rest of this paper is structured as follows: In Section 2, the component-level state estimations and related flowcharts and algorithms are briefly explained. The focused approach of the paper for state estimation at the system level is described in Sections 3–5. In Section 3, the estimation of the SoF of the EV is discussed. Section 4 deals with the simulation model of the EV and related kinematics for the estimation of the road-load power demand. In Section 5, the derating schemes are presented, and the design and implementation of the proposed recommender system in the STATEFLOW© are obtained. The simulation results of the proposed recommender system are provided and discussed in Section 6. Finally, in Section 7, the paper is concluded.

2. Component-Level State Estimation

This section discusses the utilized algorithms for state estimation at the component level, and a hybrid battery–supercapacitor ESS was considered as the use case. The usefulness of hybrid storage systems in the automotive context has been demonstrated in a large body of work, e.g., [28,29].

The block diagram of the EV drivetrain, including the ESSs, motor drive, DC–DC converters, electrical motor, ECU, etc., is shown in Figure 1. As seen, it was assumed that the EV is powered using a hybrid ESS, which is a combination of the battery and supercapacitor, a three-phase two-level inverter, and a permanent-magnet synchronous motor (PMSM). The hybrid ESS usually requires an interfacing power electronics converter to connect the battery and supercapacitor. A complete review of different topologies for hybrid ESSs can be found in the authors' previous work [5]. It was also assumed that in the hybrid ESS, the battery and supercapacitor are both connected to the DC link of the motor drive through two different bidirectional DC–DC converters. This structure provides excellent flexibility for sharing power between the individual ESSs during the acceleration or regenerative braking of the EV. This topology was used as an example, but the proposed concept must similarly work for other topologies. For example, an alternative topology can be to directly connect the battery to the DC link, and the supercapacitor bank can be interfaced with the DC link via a DC–DC converter. To build upon our previous work and facilitate the simulation work, we have considered converter monitoring techniques proposed in our earlier papers [21,23,30]. Nevertheless, other SoP estimation algorithms can be used for the component-level estimation phase.

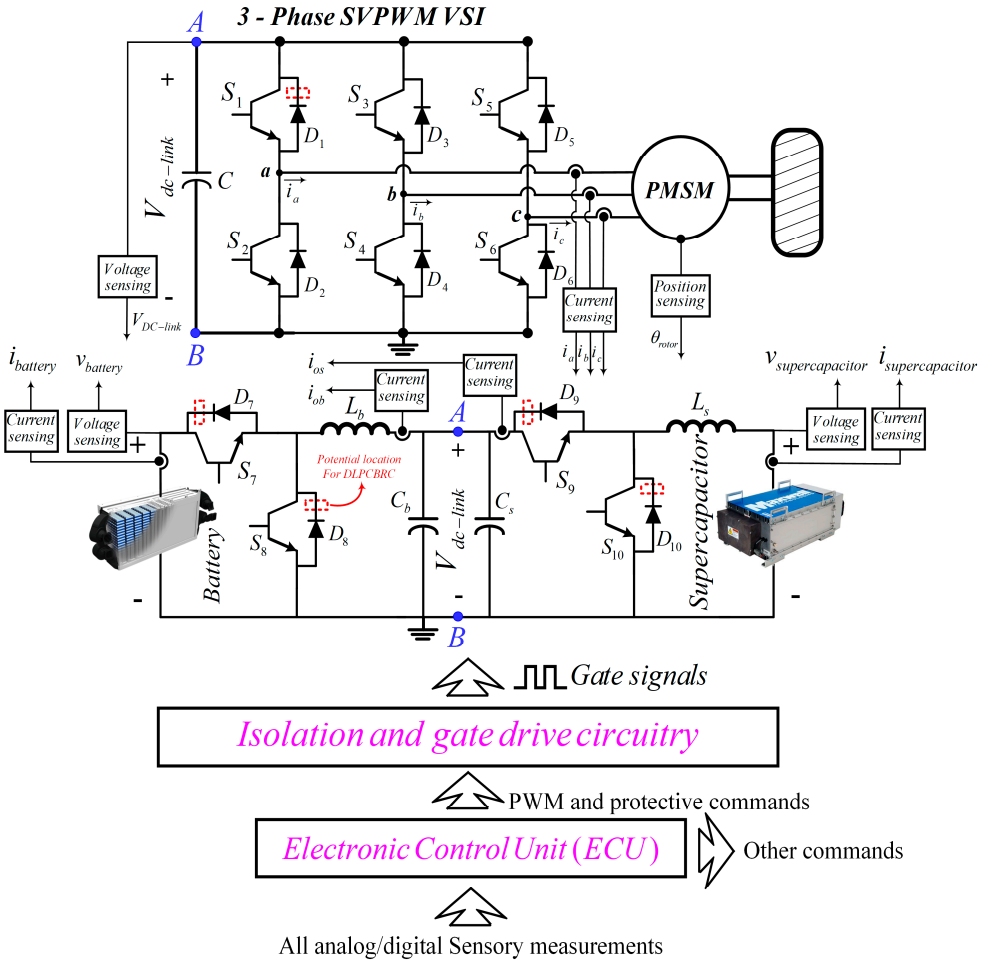

Figure 1. Electrical block diagram of the EV drivetrain.

In addition, it was assumed that the battery has a higher voltage profile, and the supercapacitor has a lower voltage profile than the voltage of the DC link. Therefore, the buck-boost converter of the battery is connected such that it works in the buck mode during normal operation mode, and it will be operated in the boost mode when the EV is braking (or coasting) to harvest the regenerative braking energy. On the other hand, the supercapacitor converter operates in the boost mode during normal operating modes and switches to the buck mode during braking (or coasting) occasions.

All estimation algorithms were embedded in the ECU of the EV. The core element of the ECU is a microcomputer with a processing capability reaching 2.5 GHz (an example is Tesla's AMD Ryzen YE180FC3T4MFG with 2.8 GHz), which enables real-time parallel execution of different sophisticated estimation algorithms. The ECUs are also equipped with Flash, SRAM, and EEPROM memories, which enable downloading bulky codes in the ECU and buffering a large amount of data during the execution of the codes. The ECU also comes with embedded input/output (I/O) digital and analog channels for the supply, reading of the sensory measurements, control commands for the drive and actuators, etc. The sensory measurements in the whole EV drivetrain include the voltage and current of the batteries and supercapacitors, PMSM three-phase currents, voltage and current measurements of the DC–DC converters, rotor position reading by the encoder (or three-phase Hall-effect sensors), DC-link voltage, reference speed and commands from the acceleration and braking pedals, inverter signals, the output voltage of the Rogowski Coils (please refer to [23] regarding the method for power-loss estimation algorithm), the linear speed of the EV through speed sensor, road angle through gyroscope, etc.

In Figure 1, $V_{DC-link}$ is the DC-link voltage; $i_{battery}$ and $v_{battery}$ are the current and voltage of the battery ESS; $i_{supercapacitor}$ and $v_{supercapacitor}$ are the current and voltage of the supercapacitor ESS; i_a, i_b, and i_c are the motor phase currents; i_{os} and i_{ob} are the converter currents; S_1-S_{10} and D_1-D_{10} are the IGBT switches and diodes in the converters; C denotes the DC-link capacitance; L_b and L_s denote the converter inductances; and θ_{rotor} is the rotor position in the PMSM. The voltage-source inverter (VSI) is operated based on the space-vector pulse-width modulation (SVPWM).

The following subsections introduce algorithms that were used to obtain the component-level state estimation.

2.1. Supercapacitor and Battery SoP Estimation and Monitoring

Concerning the supercapacitor ESS, two existing estimation algorithms were used: 1—the method proposed in [25], wherein a co-estimation algorithm based on the supercapacitor nonlinear model (three-branch RC ECM) and UKF was used for joint accurate estimation of state-of-health (SoH) and SoC, and 2—the method presented in [27], wherein a linear supercapacitor model and a recursive extended least-squares (RELS) algorithm were used for obtaining an estimation of aging parameters for diagnosis purpose only. As shown in Figure 2, the two estimation algorithms run in parallel but with different sample times for SoH and SoC estimations. The estimated SoH and SoC are then combined with the SoP estimation method presented in [17] to estimate the dynamic power limits of the supercapacitor. The SoP of the supercapacitor determines the maximum available discharge power that can be safely released to the drivetrain.

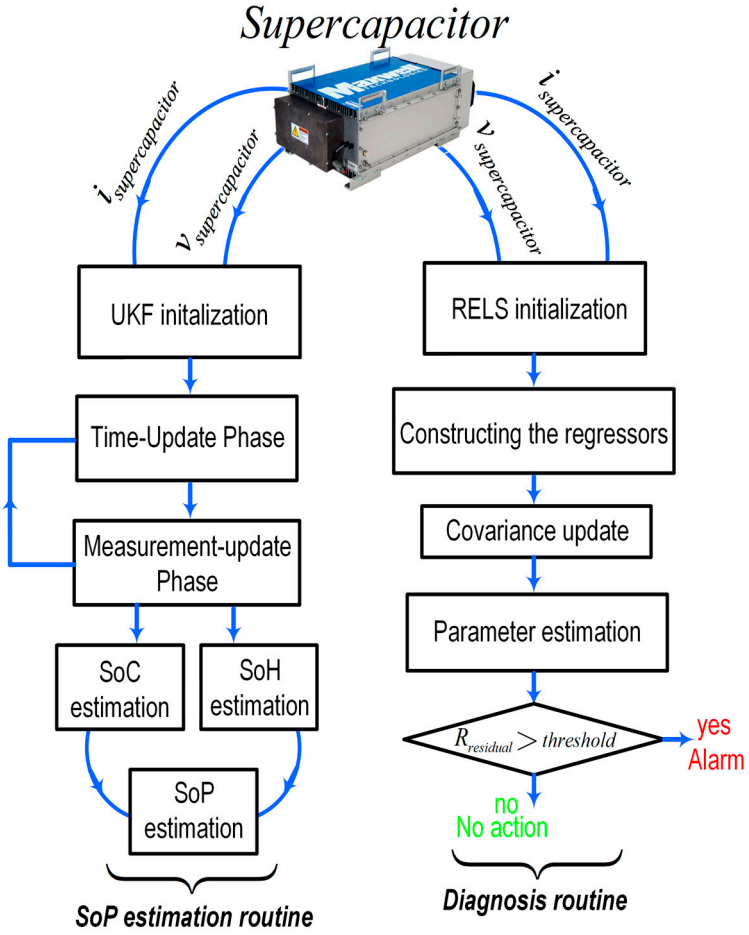

Figure 2. SoF estimation and diagnosis of the supercapacitor in the AEV.

In the case of the battery ESS, the critical states, including the battery SoC, SoH, and SoP were co-estimated using the EKF and RLS algorithms, as described in detail in [31]. For

SoC and SoH estimation, a large number of studies have been done, which can be reused in this context [32].

2.2. Performance Monitoring of the Converters

Normally, the DC–DC converters and motor drives in the EV drivetrain are sized according to the maximum power that can be supplied by the ESSs. The systems are usually designed to tolerate a certain level of overload. However, there exist several conditions under which the components might not be able to reach their expected performance characteristics, e.g., due to aging, cooling problems, or failures. For example, in certain driving conditions, such as driving at a high altitude and temperature (where the cooling system becomes less efficient) with maximum road load conditions, the components might not be able to work as they are expected to. Therefore, it is probable that the power electronics circuits cannot handle the maximum available power of the ESSs. In this regard, a determining factor is the junction temperature of the semiconductor switches. When the junction temperature reaches a maximum safety threshold, a protection signal is sent to the motor drive to take immediate safety action (note that this is apart from the short-circuit condition, which requires more sophisticated protection methods). Therefore, the motor drive should be derated according to the estimated junction temperature to keep the power module in a safe operating region (a safety region before the maximum threshold must be usually maintained for safety reasons). The utilized derating scheme determines the SoP of the motor drive, i.e., it determines the maximum power that can be handled by the motor drive for energizing the PMSM. In this paper, it was assumed that the EV is equipped with a PMSM controlled with a SVPWM-field-oriented control (FOC) and a fixed switching frequency. The junction temperature can be reduced by decreasing the power losses of the power modules (to mitigate heating the modules) by either lowering the switching frequency or reducing the load power. In this regard, for example, the active thermal control approach proposed in [33] can be used. However, since thermal control is not within the scope of this work, we only assumed that the motor drive is 100% functional when its junction temperature is below the derating level. Otherwise, the motor drive would linearly be derated by 1% for each degree Celsius above the derating level (a similar approach has been used by Hyundai Motors© [34]). However, it would be worthwhile to take advanced derating schemes into account for the estimation of the motor drive SoF. In addition to junction temperature estimation, an effective open-circuit fault (OCF) or open-switch fault (OSF) diagnosis method, which is based on the authors' previous contributions, was considered in this paper. The diagnosis algorithm runs in parallel with the temperature estimation subroutine for the monitoring of the power module. The flowchart of the whole algorithm for the power module is depicted in Figure 3.

2.3. Derating of the PMSM

Contrary to the motor drive and DC–DC converters, which are composed of sensitive IGBT modules with fast temperature rise time, the thermal time constants of the electrical PMSMs are relatively high. Even in overload or harsh conditions, the temperature in the windings of the PMSM will not suddenly increase (the thermal constant of the PMSM depends on the size of the motor and its insulation class). Therefore, the PMSM is not often a limiting component in converting the ESSs' electrical power to the required mechanical torque. Nonetheless, it is necessary to derate the PMSM under certain circumstances, e.g., when the cooling system is not effective due to aggressive operating conditions such as very high temperatures or high altitudes, which result in low air pressure. Currently, many of the PMSM manufacturers provide the derating information versus the temperature and altitude for different motors sized from 1 to 200 horsepower in their application manuals. For instance, Table 1 shows the amplitude and ambient reduction factors for SIEMENS© electrical motors. In our work, this information was simply incorporated as a 3-D lookup table for real-time estimation of the SoP of the PMSM.

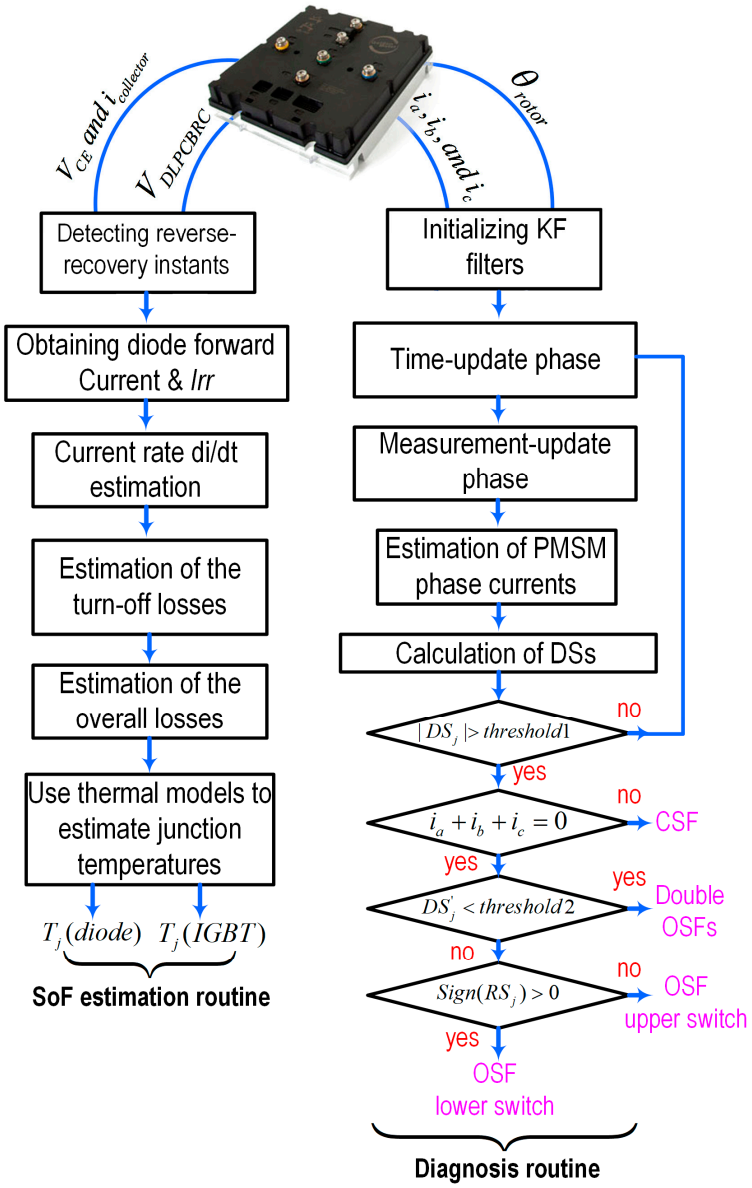

Figure 3. SoP estimation and diagnosis of the motor drive in the EV based on the authors' previous contributions in [21,23].

Table 1. Derating factor versus different levels of ambient temperature and altitude (taken from SIEMENS© motor application manual).

Altitude Above Sea Level (Meters)	Ambient Temperature						
	30 °C	35 °C	40 °C	45 °C	50 °C	55 °C	60 °C
1000	1.06	1.03	1.00	0.96	0.92	0.87	0.82
1500	1.03	1.00	0.97	0.93	0.89	0.84	0.80
2000	1.00	0.97	0.94	0.90	0.86	0.82	0.77
2500	0.95	0.93	0.90	0.86	0.83	0.78	0.74
3000	0.91	0.89	0.86	0.83	0.79	0.75	0.71
3500	0.87	0.84	0.82	0.79	0.75	0.71	0.67
4000	0.82	0.79	0.77	0.74	0.71	0.67	0.63

3. System-Level Estimation of the SoF

As mentioned before, the main contribution of this work is to extend the definition of the SoF for the whole EV drivetrain by concurrently considering all components. Real-time knowledge of the SoF of the EV helps the driver to understand the overall functionality of the EV and to realize whether the EV can meet certain driver demands and real-time road load requirements. This information can affect drivers' decisions to provide safer driving conditions. The SoF of the EV depends on the type of energy management strategy used to control the power flow of the individual ESSs, e.g., battery and supercapacitor. To consider the worst-case design boundary, it was assumed that the battery and supercapacitor-related control systems are configured such that they can simultaneously provide their maximum available power to the EV drivetrain. The SoF of the EV can then be estimated taking the estimated SoFs of all system components (as fulfilled in the component-level estimation) into account as follows:

$$SoF_{AEV} = min\left\{\left(P_{SC,max}^{discharge} + P_{Battery,max}^{discharge}\right), DF_{drive} \times P_{Drive,max}, DF_{motor} \times P_{PMSM,rated}\right\} \quad (1)$$

where SoF_{AEV} is the overall SoF of the EV; $P_{SC,max}^{discharge}$ is the maximum available power by the supercapacitor (obtained by estimating the supercapacitor SoP); $P_{battery,max}^{discharge}$ is the maximum available power of the battery (obtained by estimating the battery SoP); DF_{drive} is the derating factor of the motor drive; $P_{drive,max}$ is the rated power of the motor drive; DF_{motor} is the derating factor of the PMSM; and $P_{PMSM,rated}$ is the rated power of the PMSM. In (1), the SoF of the EV is estimated taking into account the ESSs, electrical motor, and motor drive. In addition, the SoF is estimated without considering the power losses associated with the transmission system and electrical motor. In practice, the foregoing factors can also be considered by obtaining and taking into account the efficiency map of these components.

4. Road Load and Traction Forces of the EV [5]

In this Section, the real-time road load requirements (dynamic tractive requirements) were estimated using a 2-D model of the vehicle kinematics [35]. This model represents the driving forces of the vehicle as shown in Figure 4.

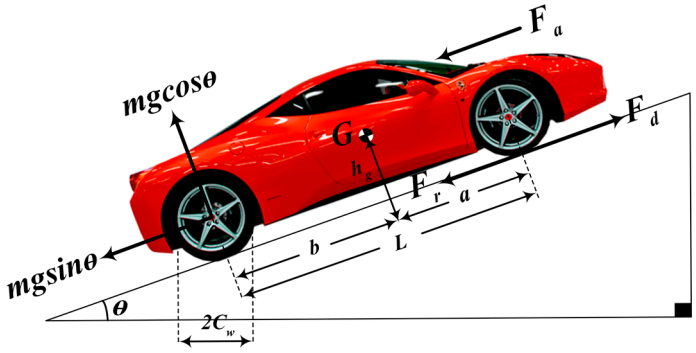

Figure 4. Forces acting against the EV during driving and two-axle braking dynamics of the EV [5].

Generally, these forces can be categorized into four categories as follows:

4.1. Rolling Resistance Losses

This is the force required against the friction between the tires and the road (known as rolling resistance) and has been represented in the literature by:

$$F_r = K_r mg\cos\theta \quad (2)$$

In (2), K_r is the rolling resistance coefficient; m is the mass of the EV and payload (kg); θ is the slope angle (degree); and g is the gravitational constant (m/s^2).

4.2. Aerodynamics Resistance Losses

Aerodynamic losses are produced as a result of the friction between the airstream and the EV body. Aerodynamic resistance is modeled as:

$$F_a = \frac{1}{2}\rho C_d A_f v^2 \tag{3}$$

In (3), ρ is the air density (kg/m^3); C_d is the coefficient of drag force; A_f is the frontal area of the vehicle (m^2); and v is the linear velocity of the EV (m/s^2).

4.3. Road Gradient Force

The road gradient force can be written as follows:

$$F_g = mg\sin\theta \tag{4}$$

4.4. Transient Force

Transient force is required to accelerate or decelerate the vehicle and can be written as $m\frac{dv}{dt}$. Based on the forces calculated, the required total force can be written as follows:

$$F_d = F_r + F_g + F_a + m\frac{dv}{dt} \tag{5}$$

Substituting (2)–(4) in (5) yields:

$$m\frac{dv}{dt} = F_d - K_r mg\cos\theta - \frac{1}{2}\rho C_d A_f v^2 - mg\sin\theta \tag{6}$$

In (6), F_d is the supplied force by the vehicle engine to drive the car as follows:

$$F_d = m\frac{dv}{dt} + \underbrace{K_r mg\cos\theta + \frac{1}{2}\rho C_d A_f v^2 + mg\sin\theta}_{\text{resistive forces}} \tag{7}$$

The tractive force is transformed into the tractive torque using $T_d = F_d \times r_{wheel}$, where r_{wheel} is the wheel's radius. Finally, the PMSM torque can be obtained by taking the gear ratio into account as follows:

$$T_{motor} = T_d/(gear\ ratio) \tag{8}$$

5. Design of the Proposed Recommender System in STATEFLOW©

In the previous section, the road load requirements and dynamic tractive forces of the EV were derived. The output of the accelerator pedal determines the reference speed. In addition, the rate of change of the position of the accelerator pedal, which shows how fast the pedal is depressed, determines the acceleration of the EV. Based on this input and using (2)–(8), the electrical torque (T_{demand}) and power (P_{demand}) that are needed by the EV can be calculated. On the other hand, the estimated SoF of the EV determines the maximum power that potentially can be supplied by the drivetrain without exceeding any of the safety thresholds of the components. Whenever $P_{demand} < SoF_{AEV}$, the EV can reach the setpoint requested by the driver without any problem. However, when $P_{demand} > SoF_{AEV}$, the EV cannot meet the road load requirements, and the components of the EV will also be subjected to severe overload conditions and may exceed their critical safety thresholds. Two problems may arise here. First, the driver could expect successful EV maneuverability in certain driving conditions (e.g., expecting a certain acceleration level during overtaking), which cannot be fulfilled due to the low drivetrain SoF, and thus, safety can be compromised. Hence, it is necessary to inform the driver of the low drivetrain SoF to avoid an unsuccessful maneuver (e.g., overtaking). Second, components of the driv-

etrain could exceed their safe operating limits. Therefore, according to the real-time SoF of the EV and the driver commands, the EV should be derated by some means. In this paper, two derating schemes were proposed to achieve the foregoing goals. In the following, first, these derating schemes are explained. The SoF estimation subroutines and the derating schemes were implemented in an online recommender system using STATEFLOW© in MATLAB.

5.1. Derating Scheme 1: Adaptive Cruise Control (ACC)

Adaptive cruise control (ACC) is an already available cruise control system for road vehicles. This system automatically adjusts the vehicle speed for maintaining a safe distance from other vehicles ahead [36]. In this work, it is suggested to expand the ACC system concept to adjust the cruising speed such that not only the safety distance is maintained (similar to the traditional ACC system), but also the new cruising speed provides a safer operating regime for the EV components. Accordingly, a new ACC system is herein proposed. In the proposed scheme, the new cruising speed is selected by considering the real-time SoF of the EV. In the proposed ACC system, the cruising speed is confined by the maximum achievable cruising speed ($v_{cruising}^{limit}$) of the EV, which can be determined using the estimated SoF in Section 3. The maximum power of the EV drivetrain can be obtained by first subtracting the approximated losses of the motor drive and electric motor from the SoF of the EV, i.e., SoF_{AEV}. The power losses of the motor drive were already estimated in the component-level stage. The power losses of the electric motor can be obtained indirectly, by obtaining the PMSM efficiency map with offline experimentations (it is herein skipped for simplicity considering that the PMSM efficiency is >97%). The maximum output power of the EV drivetrain can then be obtained as follows:

$$P_{PMSM,net} = SoF_{AEV} - P_{drive,loss} - P_{PMSM,loss} \tag{9}$$

where $P_{drive,loss}$ and $P_{PMSM,loss}$ are the power losses of the motor drive and PMSM, respectively. The maximum torque that can be generated at each instant can be calculated using the following formula:

$$T_{PMSM,net} = \frac{P_{PMSM,net}}{\omega_{rotor}} \tag{10}$$

Considering the gear ratio of the transmission system, the value of the torque at the wheels of the EV can be obtained as follows:

$$T_d^{\max} = T_{PMSM,net} \times gear\ ratio \tag{11}$$

Finally, the maximum available tractive force can be calculated as follows:

$$F_d = \frac{T_d}{r_{wheel}} \tag{12}$$

Based on (7), the maximum achievable cruising speed can be derived as follows:

$$\begin{aligned} &F_d = \underbrace{m\frac{dv}{dt}}_{0} + K_r mg\cos\theta + \frac{1}{2}\rho C_d A_f \left(v_{cruising}^{limit}\right)^2 + mg\sin\theta \Rightarrow \left(v_{cruising}^{limit}\right)^2 = \\ &\frac{2\left(F_d - K_r mg\cos\theta - mg\sin\theta\right)}{\rho C_d A_f} \Rightarrow v_{cruising}^{limit} = \sqrt{\frac{2\left(F_d - K_r mg\cos\theta - mg\sin\theta\right)}{\rho C_d A_f}} \end{aligned} \tag{13}$$

The flowchart of the proposed ACC system is shown in Figure 5. This driving mode can be recommended to the driver when the cruise control mode is already activated. When the cruise control mode is not activated, the required tractive force is determined by the driver's command (through acceleration pedal input). In such conditions, the EV can be derated by defining a virtual pedal position as proposed in the next Section.

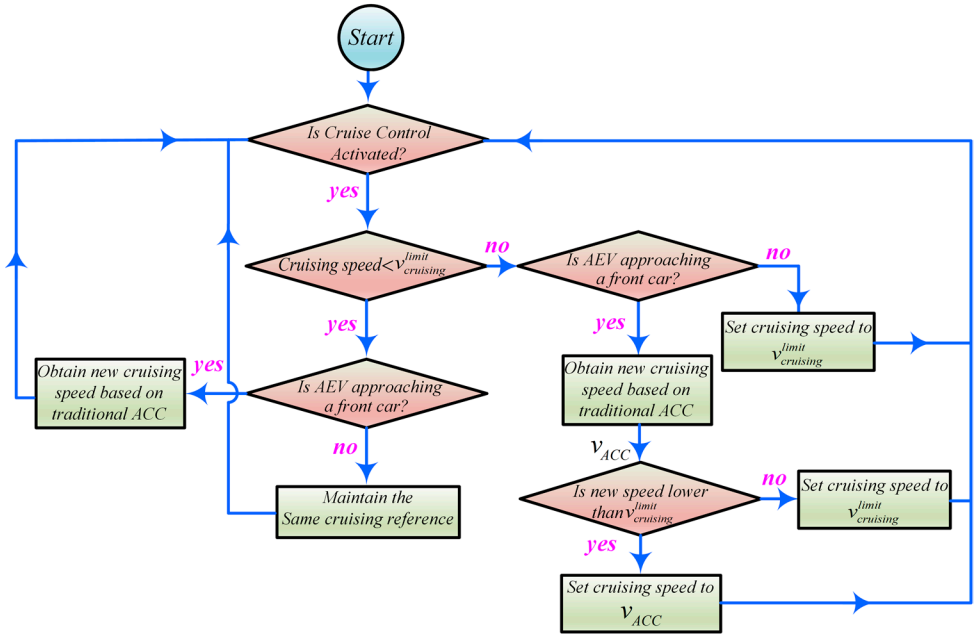

Figure 5. Flowchart of the proposed ACC system.

5.2. Derating Scheme 2: Adaptive Pedal Sensitivity Adjustment (APSA)

Peak power transient conditions usually take place during the acceleration of the EV. Therefore, when the estimated SoF_{AEV} is relatively low, such transient conditions can subject all system components to safety risks. To resolve this issue, in this section, an Adaptive Pedal Sensitivity Adjustment (APSA) mode is proposed. In the proposed design, first, the maximum achievable cruising speed $v_{cruising}^{limit}$ is obtained using (13). According to the obtained cruising speed, a virtual pedal position filter is defined to confine the speed reference command by the driver. Second, the maximum achievable EV acceleration is calculated, and accordingly, the pedal sensitivity is adaptively limited using a rate limiter filter. Therefore, a new operating mode herein defined as the "safe mode" was designed. Calculation of $v_{cruising}^{limit}$ was explained in the previous subsection. The maximum achievable acceleration can also be obtained considering (7) as follows:

$$\begin{array}{c} F_d^{\max} = m\left(\frac{dv}{dt}\right)_{\max} + K_r mg\cos\theta + \frac{1}{2}\rho C_d A_f v^2 + mg\sin\theta \Rightarrow \\ \left(\frac{dv}{dt}\right)_{\max} = \frac{F_d^{\max} - K_r mg\cos\theta - \frac{1}{2}\rho C_d A_f v^2 - mg\sin\theta}{m} \end{array} \quad (14)$$

According to (14), a pedal filter was designed, which obtains a virtual pedal position such that the safety of the EV components based on its real-time SoF_{AEV} will be guaranteed. The rate-limiting concept is shown in Figure 6.

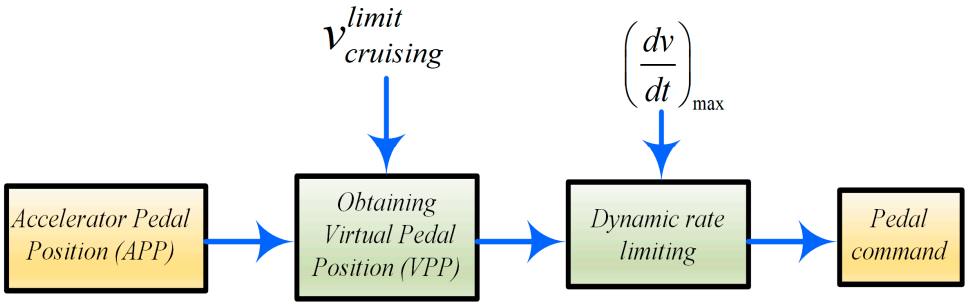

Figure 6. The proposed APSA scheme.

5.2.1. Virtual Pedal Position (VPP)

In the proposed safe mode, the VPP can be obtained by a linear filter considering the maximum achievable cruising speed, as shown in Figure 7. It is assumed that the accelerator pedal travels 30 degrees at maximum depression. The linear filter can be easily obtained by writing the equation of the straight line AB in Figure 7.

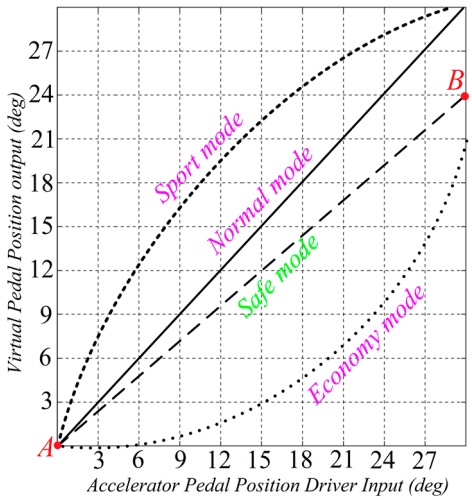

Figure 7. Real versus virtual accelerator pedal position in different operating modes.

In practice, the location of point B in Figure 7 depends on $v_{cruising}^{limit}$. The linear filter can then be obtained as follows:

$$A(0,0)\,,\; B\left(30, \frac{30 \times v_{cruising}^{limit}}{v^{\max}}\right) \Rightarrow VPP = \frac{v_{cruising}^{limit}}{v^{\max}} APP \tag{15}$$

5.2.2. Dynamic Rate Limiting

Based on (14), a dynamic rate limiter was adopted to lower the change rate of the VPP in the proposed safe operating mode. The rate limiter limits the first derivative of the VPP to be no faster than the specified value obtained in (14). The derivative is calculated using the following equation:

$$rate = \frac{u(k) - y(k-1)}{t(k) - t(k-1)} \tag{16}$$

where $u(k)$ and $t(k)$ are the current input and time, and $y(k-1)$ and $t(k-1)$ are the output and time from the previous step. The output is determined by comparing the signal rate to $\left(\frac{dv}{dt}\right)_{max}$. If the rate is lower than $\left(\frac{dv}{dt}\right)_{max}$, the same input will be sent to the output. Otherwise, if the rate is larger than $\left(\frac{dv}{dt}\right)_{max}$, the output is calculated as follows:

$$y(k) = \Delta t \times \left(\frac{dv}{dt}\right)_{\max} + y(k-1) \tag{17}$$

5.3. Implementation of the Proposed Recommender System Using STATEFLOW©

STATEFLOW© is a powerful graphical design and development tool for complex control and supervisory logic problems. Previously, well-known car manufacturers have used STATEFLOW© in the ECU design stage. For instance, Tesla Roadster, Volvo, and Fiat Chrysler Automobiles are among car manufacturers that have used STATEFLOW© in the ECU design stage. Therefore, due to its wide acceptance, in this paper, STATEFLOW© was chosen for the implementation of the proposed schemes and the online recommender system.

The proposed scheme is suggested to be implemented as an add-on or subroutine to the traditional ADASs [37,38]. Therefore, similar to other ADASs, the proposed recommender system can take advantage of advanced technologies such as automatic speech recognition (ASR) [39], text-to-speech (TTS) modules, spoken dialog system (SDS), information filter, and user profile database. The proposed recommender system can communicate with the EV systems via a multiplex network such as a controller area network (CAN).

The proposed recommender system first performs real-time state estimation based on the sensory measurements and techniques explained in the previous sections. Then, it obtains the real-time SoF of the EV and collects supplementary sensory data related to the road and environmental conditions. Based on the estimated SoF of the EV and approximated road load dynamic requirements, the recommender system may change the powertrain performance mode, for instance, between the sport mode, normal mode, fuel economy mode, or the proposed safe mode. The recommender system changes the operating mode based on the preferences of the driver, communicated and confirmed through voice commands, for example. The proposed recommender system has a proactive performance mode advisory function, which recommends either of the foregoing performance modes to the driver according to the observation of recent driver actions. The advisory commands are constructed based on the data collected from the vehicle or non-vehicle sources. The knowledge of the driver's past actions, behavior, and preferences might also be considered in constructing the advisory commands (though it was not considered here). The proposed safe mode informs the driver that the current SoF of the EV is not sufficient to meet the road load requirements based on the driver's pedal command. Thus, it suggests switching to safe mode for maintaining the safety of the EV and warns the driver to consider caution in his/her decisions. In the traditional fuel economy mode, the powertrain will be configured to enhance the fuel economy with some potential degradation in the acceleration performance, as seen in Figure 7. On the other hand, the sport mode increases acceleration and EV responsiveness. In addition, the normal mode is an intermediate mode, which is configured to balance the EV fuel economy and the acceleration performance attributes. The proposed recommender system can use verbal interaction between the driver and the EV to avoid hazards of look-away events, to make the recommender system easy to use, and preferably, to save space on the dashboard. In the proposed safe mode, estimation of the SoF of the EV can be completed in regular intervals, taking into account the required computational load. When the recommended mode differs from the current mode, the proposed recommender system may initiate a verbal exchange with the driver of the car. For instance, if a safe mode or ACC mode is decided by the recommender system, it can create a text string containing the words that the driver should hear, such as, "would you like to switch to the safe mode?" or "would you like to switch to the ACC mode?" The recommender system can continue to explain, "I think the car might work in a safer condition." The text string can be sent to the TTS module, and the SDS system then waits for a response from the driver. Upon hearing the words, the driver formulates a response, which can be "yes" or "no," but also can be something more unexpected, such as, "What is the safe mode" or "What is the ACC mode" or "Ask me later," etc. Upon receiving a confirmation from the driver, the recommender system activates, e.g., the safe mode, and sends a text string containing the sentence, "Safe driving mode activated," to the TTS module. The information filter ensures that interactions with the driver take place only at appropriate times, e.g., when a driver response is necessary (in critical or fault conditions), when the driver can make a decision (for example recommender avoids interacting with the driver in certain driving conditions, such as passing a cross-road or when the driver is taking a turn). The information filter is responsible for making sure that the recommendations are not made too frequently, causing distraction, frustration, or dissatisfaction with the recommender system. The recommender system can be deactivated by the driver when he/she prefers. In either of the operating modes, when a fault arises in the components of the EV drivetrain, which can be detected by the diagnosis subroutines developed in the previous sections, the recommender system immediately informs the driver to take precautionary actions.

In the previous paragraphs, the concept of the proposed recommender system and some design suggestions and features were provided with details. In the simulation of the recommender system using STATEFLOW, however, some features such as the SDS system were not considered. For the proof of concept, it was assumed that the driver can respond to the recommender by pushing a certain button during the simulation. Nonetheless, in practice, all the aforementioned ideas and subsystems can easily be implemented on the ECU of the car. The voice commands of the recommender system were recorded, imported into the MATLAB workspace as a data file (double), and were played during STATEFLOW simulation using an interpreted MATLAB function block. The implementation view of the STATEFLOW block diagram of the proposed recommender system is shown in Figure 8. As shown in Figure 8, the finite state machine included four state blocks that represent different drivetrain components, a state block for the representation of the drivetrain SoF, and a state block for the recommender system. The state machines of the components included a Simulink function that executes the corresponding state estimation algorithms. Every state block had a parent state and offspring states. Transitions were also placed to move from one state to another depending on the drivetrain SoF and the operating conditions.

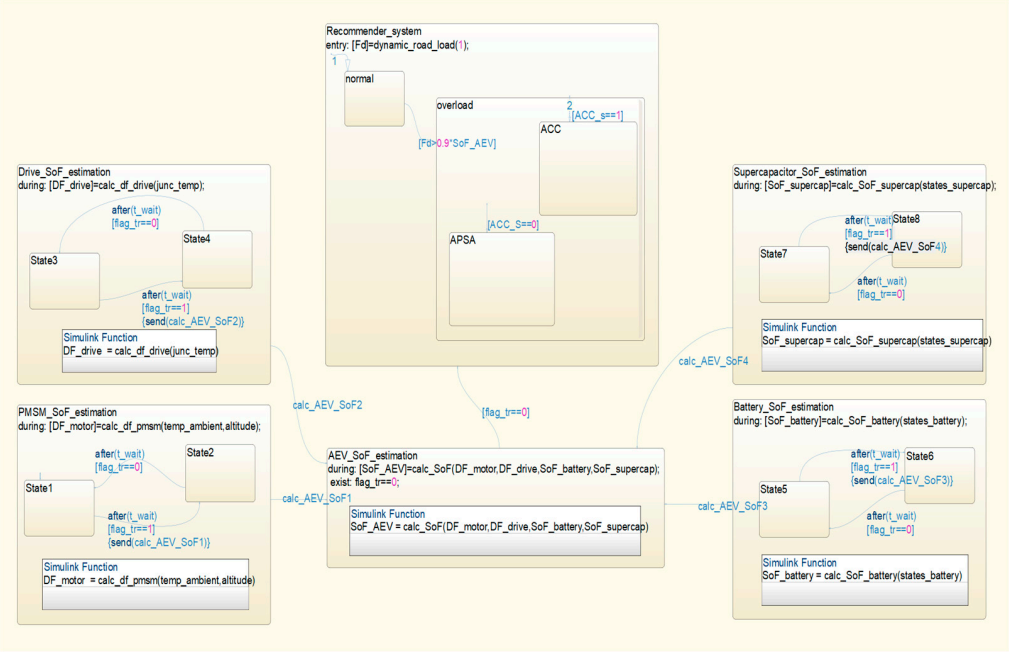

Figure 8. An overview of the implemented recommender system in STATEFLOW©.

6. Simulation Results

This section describes the simulations using MATLAB/SIMULINK and STATEFLOW© conducted to confirm the effectiveness of the proposed recommender system. The drivetrain of the simulated EV consisted of a hybrid ESS with a 96 V, 30 kWh lithium-ion battery pack, and a supercapacitor bank consisting of 90 (24×12) 2.5 V, 2500 F supercapacitor cells (MAXWELL PC2500). The IGBT module was based on the power module from Fuji. The electrical motor model was an MC-PM8 from ADVISOR [40]. Other simulation parameters of the EV were selected based on VEH_SMCAR from the ADVISOR software. The EV mass with cargo was 1144 kg; the frontal area was 2 m^2; and the radius of the wheels was 0.335 m. Detailed simulation parameters are listed in Table 2. The PMSM motor drive was controlled with the FOC method, which is the SotA approach for speed control and has been recently considered in many EVs. The FOC decouples torque and flux by using a d-q rotor reference frame. The standard drive cycle output was considered to be the driver request during the simulations.

Table 2. Simulation parameters for testing the recommender system.

Parameter	Value
Air density	ρ = 1.2 kg/m^2
Gravitational constant	g = 9.8 m/s^2
Slope angle	$\theta = 0$ degrees
Frontal area of the AEV	A_f= 2 m^2
Radius of the wheel	$r_{wheel} = 0.335$ m
AEV mass with cargo	1144 kg
Coefficient of rolling resistance	$K_r = 0.009$
AEV model	ADVISOR VEH_SMCAR
PMSM	ADVISOR MC_PM8
Battery	Li-ion 96 V, 30 kWh
Supercapacitor	60 V, 1250 F
SVPWM frequency	10 kHz
Drive cycle	US06
Average speed	77.9 km/h
Maximum speed	128.91 km/h
% of time cruising	25.67%
% of time accelerating	36.24%

In Figures 9–11, the simulation scenarios and results with and without the utilization of the proposed recommender system are depicted.

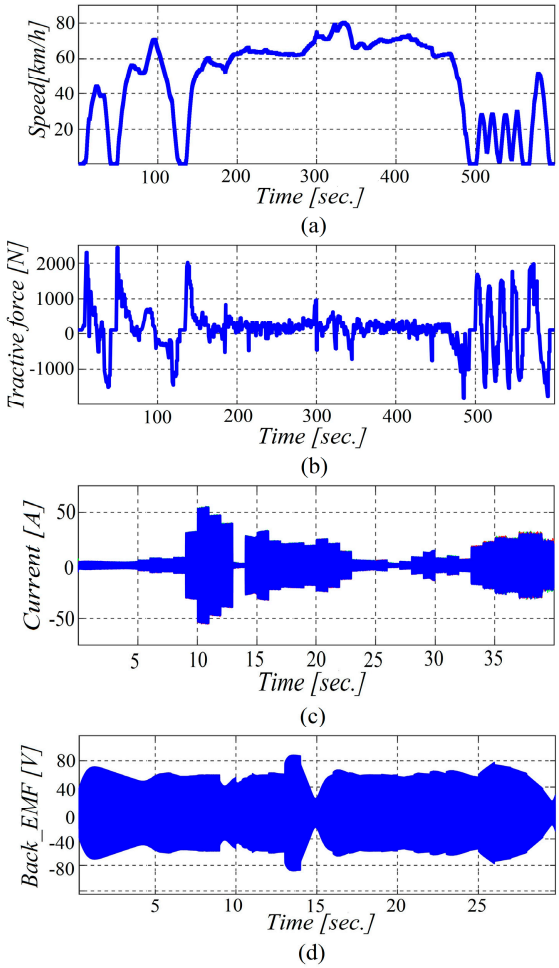

Figure 9. Simulation results without the utilization of the proposed recommender system. (**a**) Waveform of the US06 drive cycle (**b**) tractive requirements (**c**) PMSM Phase current (**d**) PMSM back-EMF.

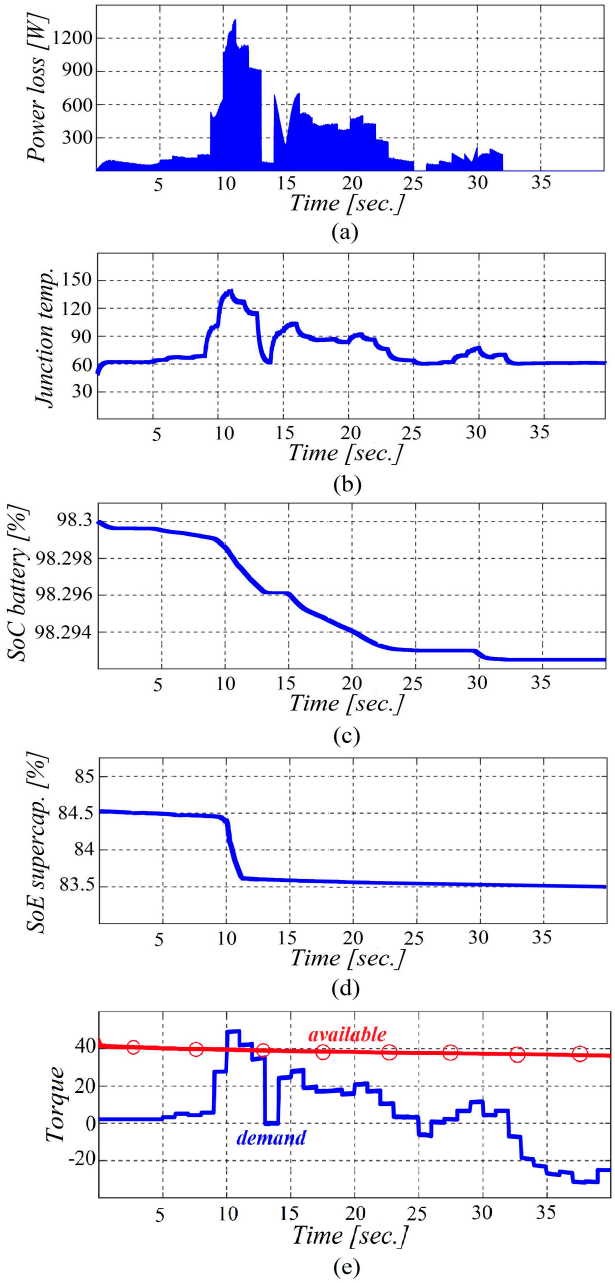

Figure 10. Simulation results without the utilization of the proposed recommender system (when the driver rejects the request of the recommender system) (**a**) Total power losses of the IGBT module (one switch) (**b**) Estimated junction temperature (**c**) Estimated battery SoC (**d**) Estimated supercapacitor SoC (**e**) Available and demanded tractive torque.

The selected drive cycle was US06, which lasts for $\Delta t = 583$ s and includes 25.67% cruising events and 36.24% acceleration events. It must be noted that due to the heavy computational burden of the simulation model (since many of the control and estimation algorithms run at the same time), only a small portion of the US06 drive cycle was simulated. The transient force diagram of Figure 9b shows that the peak power demands occur only during the acceleration events. For instance, while the average required transient force is about 200 N during cruising conditions, e.g., between $200 < t < 300$, the required transient force reaches values as large as 2000 N during the acceleration of the EV. Based on Figure 9c, the current waveform also experiences a large overshoot during the acceleration events. The waveform provided in Figure 10b also indicates that the junction temperature of the power module was correctly monitored over the simulation course.

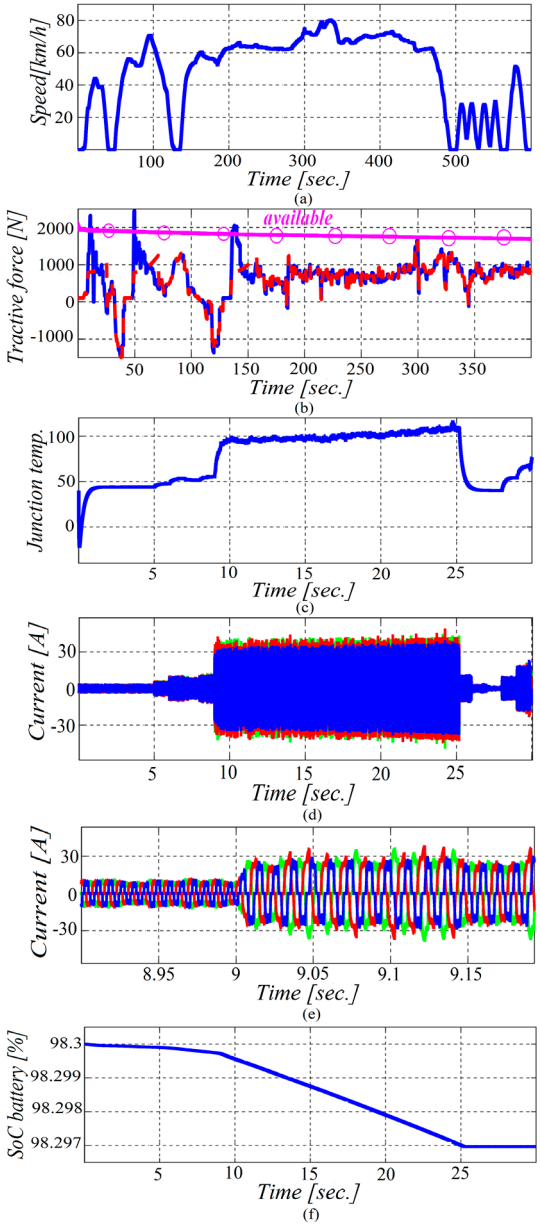

Figure 11. Simulations results with the proposed recommender system (when the driver switches to the safe mode upon request of the recommender system) (**a**) Speed profile during the driving cycle (**b**) Tractive force of the EV (**c**) Junction temperature of the power module (**d**) Motor current (**e**) Zoomed view of the motor current (**f**) SoC of the battery.

In addition, it is evident that between $t = 10$ s and $t = 12.5$ s, the junction temperature had exceeded the critical safety threshold of 120 degrees Celsius. The demanded torque and the available torque (obtained by estimation of the SoF of the EV) are also shown in the last plot in Figure 10e. It can be seen that between $t = 10$ s and $t = 12.5$ s, the demanded torque had exceeded the available torque, and thus, the motor drive junction temperature had exceeded its critical limit. In this scenario, the recommender system successfully issued the recommendation to switch to the safe mode, but the request was rejected by the driver. In Figure 11, the simulation results are shown for when the safe mode is activated by the driver. As seen in Figure 11b, due to the activation of the safe mode and the APSA system, the new tractive force (red plot) was reduced during the transient conditions in comparison with the previous tractive force (blue plot). Thus, as can be seen in Figure 11c, the junction temperature was effectively reduced to under 100 degrees Celsius.

7. Conclusions and Future Work

This paper presented the design of a new recommender system that can be implemented as part of the ADAS in EVs. A bottom-up approach was adopted, wherein different EV drivetrain components were studied and suitable algorithms were selected and applied to the state estimation of each component. The state estimation results at the component level were used to predict the maximum available power through the drivetrain. A new index is proposed, namely the drivetrain SoF, which decides the limits for the safe loadability of the EV drivetrain. The considered use case is an EV equipped with a hybrid ESS based on a battery–supercapacitor and a PMSM driven by an IGBT-based motor drive with SVPWM-FOC control. Within the proposed recommender system framework, the paper developed two de-rating schemes, i.e., the ACC and APSA. The proposed derating schemes were introduced to the recommender system in the form of a new driving mode, which we named the "safe mode." The recommender system continuously monitors the drivetrain and when necessary, recommends the "safe mode" to the driver. The conceptualization of the proposed system was carried out, and a simplified implementation of the recommender system was conducted using MATLAB/STATEFLOW©. The system was validated using simulation scenarios on the US06 driving cycle. For future work, it would be worthwhile to implement and test the proposed design using alternative drivetrain architectures and topologies. Future work could also focus on prototyping the proposed design to demonstrate its effectiveness through a dedicated hardware-in-the-loop setup.

Author Contributions: This paper is the result of a Ph.D. dissertation supervised by E.F. and co-supervised by P.S. Conceptualization, F.N., E.F. and P.S.; Methodology, F.N. and P.S.; Software, F.N. and S.K.; validation, F.N. and P.S.; writing, F.N. and S.K.; visualization, F.N. and S.K.; supervision, E.F. and P.S. All authors have read and agreed to the published version of the manuscript.

Funding: This research received no external funding.

Institutional Review Board Statement: Not applicable.

Informed Consent Statement: Not applicable.

Data Availability Statement: Not applicable.

Acknowledgments: The author would like to acknowledge the support received from Iran's National Elites Foundation throughout the project.

Conflicts of Interest: The authors declare no conflict of interest. The funders had no role in the design of the study; in the collection, analyses, or interpretation of data; in the writing of the manuscript; or in the decision to publish the results.

Abbreviations

Abbreviation	Definition
EV	Electric Vehicle
EU	European Commission
ICE	Internal Combustion Engine
DoD	Depth-of-Discharge
SoF	State-of-Function
SoP	State-of-Power
SoH	State-of-Health
SotA	State-of-the-Art
SoC	State-of-Charge
ECM	Equivalent Circuit Model
C-rate	Charge Rate
ECU	Electronic Control Unit
ADAS	Advanced Driver Assistant System
IGBT	Insulated Gate Bipolar Transistor
Li-ion	Lithium-ion

ESS	Energy Storage System
PMSM	Permanent-Magnet Synchronous Motor
VSI	Voltage-Source Inverter
SVPWM	Space Vector Pulse Wide Modulation
EKF	Extended Kalman Filter
UKF	Unscented Kalman Filter
FOC	Field Oriented Control
OCF	Open Circuit Fault
OSF	Open Switch Fault
ACC	Adaptive Cruise Control
APSA	Adaptive Pedal Sensitivity Adjustment
VPP	Virtual Pedal Position
CAN	Controller Area Network
ASR	Automatic Speech Recognition
TTS	Text-to-Speech
SDS	Spoken Dialog System

References

1. Naseri, F.; Karimi, S.; Farjah, E.; Schaltz, E. Supercapacitor management system: A comprehensive review of modeling, estimation, balancing, and protection techniques. *Renew. Sustain. Energy Rev.* **2021**, *155*, 111913. [CrossRef]
2. Selema, A.; Ibrahim, M.N.; Sergeant, P. Electrical machines winding technology: Latest advancements for transportation Electrification. *Machines* **2022**, *10*, 563. [CrossRef]
3. Borge-Diez, D.; Icaza, D.; Açıkkalp, E.; Amaris, H. Combined vehicle to building (V2B) and vehicle to home (V2H) strategy to increase electric vehicle market share. *Energy* **2021**, *237*, 121608. [CrossRef]
4. Last, G.; Agbro, D.E.; Asthana, A. The Future of Hybrid Electric Vehicles and Sustainable Vehicles in the UK. In *Energy and Sustainable Futures*; Springer: Cham, Switzerland, 2021; pp. 213–221.
5. Naseri, F.; Farjah, E.; Ghanbari, T. An efficient regenerative braking system based on battery/supercapacitor for electric, hybrid, and plug-in hybrid electric vehicles with BLDC motor. *IEEE Trans. Veh. Technol.* **2016**, *66*, 3724–3738. [CrossRef]
6. Saxena, S.; Roman, D.; Robu, V.; Flynn, D.; Pecht, M. Battery stress factor ranking for accelerated degradation test planning using machine learning. *Energies* **2021**, *14*, 723. [CrossRef]
7. Behi, H.; Karimi, D.; Behi, M.; Nargesi, N.; Aminian, M.; Ghanbarpour, A.; Mirmohseni, F.; Van Mierlo, J.; Berecibar, M. An Enhanced Phase Change Material Composite for Electrical Vehicle Thermal Management. *Designs* **2022**, *6*, 70. [CrossRef]
8. Shahjalal, M.; Shams, T.; Hossain, S.B.; Roy, P.K.; Jion, A.A.; Ahsan, M.; Chowdhury, J.I.; Ahmed, M.R.; Alam, S.B.; Haider, J. A numerical thermal analysis of a battery pack in an electric motorbike application. *Designs* **2022**, *6*, 60. [CrossRef]
9. Plett, G.L. High-performance battery-pack power estimation using a dynamic cell model. *IEEE Trans. Veh. Technol.* **2004**, *53*, 1586–1593. [CrossRef]
10. Tashakor, N.; Arabsalmanabadi, B.; Naseri, F.; Goetz, S. Low-Cost Parameter Estimation Approach for Modular Converters and Reconfigurable Battery Systems Using Dual Kalman Filter. *IEEE Trans. Power Electron.* **2021**, *37*, 6323–6334. [CrossRef]
11. Wang, W.; Wang, X.; Xiang, C.; Wei, C.; Zhao, Y. Unscented kalman filter-based battery SOC estimation and peak power prediction method for power distribution of hybrid electric vehicles. *IEEE Access* **2018**, *6*, 35957–35965. [CrossRef]
12. Karimi, S.; Farjah, E.; Ghanbari, T.; Naseri, F.; Schanen, J.-L. Estimation of parasitic capacitance of common mode noise in vehicular applications: An unscented Kalman filter-based approach. *IEEE Trans. Ind. Electron.* **2020**, *68*, 7526–7534. [CrossRef]
13. Naseri, F.; Schaltz, E.; Stroe, D.-I.; Gismero, A.; Farjah, E. An enhanced equivalent circuit model with real-time parameter identification for battery state-of-charge estimation. *IEEE Trans. Ind. Electron.* **2021**, *69*, 3743–3751. [CrossRef]
14. Zou, C.; Klintberg, A.; Wei, Z.; Fridholm, B.; Wik, T.; Egardt, B. Power capability prediction for lithium-ion batteries using economic nonlinear model predictive control. *J. Power Sources* **2018**, *396*, 580–589. [CrossRef]
15. Wei, C.; Benosman, M.; Kim, T. Online parameter identification for state of power prediction of lithium-ion batteries in electric vehicles using extremum seeking. *Int. J. Control Autom. Syst.* **2019**, *17*, 2906–2916. [CrossRef]
16. Yang, L.; Cai, Y.; Yang, Y.; Deng, Z. Supervisory long-term prediction of state of available power for lithium-ion batteries in electric vehicles. *Appl. Energy* **2020**, *257*, 114006. [CrossRef]
17. Naseri, F.; Farjah, E. Estimation of Supercapacitor State-of-Power in Vehicular Applications. In Proceedings of the 2021 11th Smart Grid Conference (SGC), Tabriz, Iran, 7–9 December 2021; pp. 1–5.
18. Peng, F. A novel method to estimate the maximum power for a photovoltaic inverter system. In Proceedings of the 2004 IEEE 35th Annual Power Electronics Specialists Conference (IEEE Cat. No. 04CH37551), Aachen, Germany, 20–25 June 2004; pp. 2065–2069.
19. Trintis, I.; Ghimire, P.; Munk-Nielsen, S.; Rannestad, B. On-state voltage drop based power limit detection of IGBT inverters. In Proceedings of the 2015 17th European Conference on Power Electronics and Applications (EPE'15 ECCE-Europe), Geneva, Switzerland, 8–10 September 2015; pp. 1–9.

20. Zhai, Z.; Li, C.; Li, M.; Zheng, X. Vector control of nine-phase permanent magnet synchronous motor under symmetrical fault condition for derating operation. In Proceedings of the 2020 23rd International Conference on Electrical Machines and Systems (ICEMS), Hamamatsu, Japan, 24–27 November 2020; pp. 2154–2157.
21. Naseri, F.; Schaltz, E.; Lu, K.; Farjah, E. Real-time open-switch fault diagnosis in automotive permanent magnet synchronous motor drives based on Kalman filter. *IET Power Electron.* **2020**, *13*, 2450–2460. [CrossRef]
22. Naseri, F.; Farjah, E.; Schaltz, E.; Lu, K.; Tashakor, N. Predictive control of low-cost three-phase four-switch inverter-fed drives for brushless DC motor applications. *IEEE Trans. Circuits Syst. I Regul. Pap.* **2020**, *68*, 1308–1318. [CrossRef]
23. Naseri, F.; Farjah, E.; Ghanbari, T. Application of an efficient Rogowski coil sensor for online estimation of turn-off energy loss of power diodes. *IEEE Sens. J.* **2019**, *19*, 6675–6683. [CrossRef]
24. Wang, D.; Yang, F.; Gan, L.; Li, Y. Fuzzy prediction of power lithium ion battery state of function based on the fuzzy c-means clustering algorithm. *World Electr. Veh. J.* **2019**, *10*, 1. [CrossRef]
25. Naseri, F.; Karimi, S.; Farjah, E.; Schaltz, E.; Ghanbari, T. Co-Estimation of supercapacitor states and parameters considering three-branch equivalent circuit model. In Proceedings of the 2020 11th Power Electronics, Drive Systems, and Technologies Conference (PEDSTC), Tehran, Iran, 4–6 February 2020; pp. 1–6.
26. Naseri, F.; Farjah, E.; Ghanbari, T.; Kazemi, Z.; Schaltz, E.; Schanen, J.-L. Online parameter estimation for supercapacitor state-of-energy and state-of-health determination in vehicular applications. *IEEE Trans. Ind. Electron.* **2019**, *67*, 7963–7972. [CrossRef]
27. Naseri, F.; Farjah, E.; Allahbakhshi, M.; Kazemi, Z. Online condition monitoring and fault detection of large supercapacitor banks in electric vehicle applications. *IET Electr. Syst. Transp.* **2017**, *7*, 318–326. [CrossRef]
28. Naseri, F.; Barbu, C.; Sarikurt, T. Optimal sizing of hybrid high-energy/high-power battery energy storage systems to improve battery cycle life and charging power in electric vehicle applications. *J. Energy Storage* **2022**, *55*, 105768. [CrossRef]
29. Lemian, D.; Bode, F. Battery-supercapacitor energy storage systems for electrical vehicles: A review. *Energies* **2022**, *15*, 5683. [CrossRef]
30. Naseri, F.; Farjah, E.; Ghanbari, T. KF-based estimation of diode turn-off power loss using datasheet information. *Electron. Lett.* **2019**, *55*, 1082–1084. [CrossRef]
31. Shen, P.; Ouyang, M.; Lu, L.; Li, J.; Feng, X. The co-estimation of state of charge, state of health, and state of function for lithium-ion batteries in electric vehicles. *IEEE Trans. Veh. Technol.* **2017**, *67*, 92–103. [CrossRef]
32. Naseri, F.; Schaltz, E.; Stroe, D.-I.; Gismero, A.; Farjah, E.; Karimi, S. State-of-Charge Estimation of NMC-based Li-ion Battery Based on Continuous Transfer Function Model and Extended Kalman Filter. In Proceedings of the 2021 12th Power Electronics, Drive Systems, and Technologies Conference (PEDSTC), Tabriz, Iran, 2–4 February 2021; pp. 1–5.
33. Murdock, D.A.; Torres, J.E.R.; Connors, J.J.; Lorenz, R.D. Active thermal control of power electronic modules. *IEEE Trans. Ind. Appl.* **2006**, *42*, 552–558. [CrossRef]
34. Lee, J.; Jang, H.; Shin, S.; Jang, K.; Jung, J. Over temperature protection in power module for hybrid and electric vehicle. In Proceedings of the 2016 IEEE Transportation Electrification Conference and Expo, Asia-Pacific (ITEC Asia-Pacific), Busan, Korea, 1–4 June 2016; pp. 432–435.
35. Naseri, F.; Farjah, E.; Kazemi, Z.; Schaltz, E.; Ghanbari, T.; Schanen, J.-L. Dynamic stabilization of DC traction systems using a supercapacitor-based active stabilizer with model predictive control. *IEEE Trans. Transp. Electrif.* **2020**, *6*, 228–240. [CrossRef]
36. He, Y.; Makridis, M.; Fontaras, G.; Mattas, K.; Xu, H.; Ciuffo, B. The energy impact of adaptive cruise control in real-world highway multiple-car-following scenarios. *Eur. Transp. Res. Rev.* **2020**, *12*, 1–11. [CrossRef]
37. Ball, J.E.; Tang, B. Machine learning and embedded computing in advanced driver assistance systems (ADAS). *Electronics* **2019**, *8*, 748. [CrossRef]
38. Ledezma, A.; Zamora, V.; Sipele, Ó.; Sesmero, M.P.; Sanchis, A. Implementing a gaze tracking algorithm for improving advanced driver assistance systems. *Electronics* **2021**, *10*, 1480. [CrossRef]
39. Wang, D.; Wang, X.; Lv, S. An overview of end-to-end automatic speech recognition. *Symmetry* **2019**, *11*, 1018. [CrossRef]
40. Wipke, K.; Cuddy, M.; Bharathan, D.; Burch, S.; Johnson, V.; Markel, A.; Sprik, S. *ADVISOR 2.0: A Second-Generation Advanced Vehicle Simulator for Systems Analysis*; National Renewable Energy Lab.(NREL): Golden, CO, USA, 1999.

Disclaimer/Publisher's Note: The statements, opinions and data contained in all publications are solely those of the individual author(s) and contributor(s) and not of MDPI and/or the editor(s). MDPI and/or the editor(s) disclaim responsibility for any injury to people or property resulting from any ideas, methods, instructions or products referred to in the content.